Projectile fragmentation of halo nuclei in a peripheral direct reaction model

H. Sagawa[1] and N. Takigawa[2]
[1] *Center for Mathematical Sciences, University of Aizu, Aizu-Wakamatsu, Fukushima 965, Japan*
[2] *Department of Physics, Faculty of Science, Tohoku University, Aoba, Sendai, Miyagi 980, Japan*
(Received 7 March 1994)

The transverse and longitudinal momentum distributions of projectile fragmentation of unstable nuclei are studied by using a peripheral direct reaction model. We found that the transverse momentum distribution is affected by absorptive cutoff of the fragmentation process, and the width becomes narrower than that of the longitudinal one which remains almost unaffected. The momentum distributions of fragments from unstable projectiles ^{11}Be and ^{11}Li are studied for various microscopic wave functions. Calculated results with halo wave functions show good agreement with experimental data. We discuss also the difference among various models, the spectator model, Friedman model, and Serber model, for predicting the momentum distribution.

PACS number(s): 25.70.Mn, 24.10.−i, 24.50.+g, 25.60.+v

I. INTRODUCTION

Experimental and theoretical study of unstable nuclei is currently very popular, especially in connection with developing facilities of radioactive heavy-ion beams [1]. Fragmentation reactions with secondary beams of nuclei near the drip lines are studied as a useful tool to obtain precise information of wave functions of halo nucleons [2–5]. Kobayashi *et al.* [2] extracted the separation energy and the size of halo neutrons from the transverse momentum distribution of projectile fragments without considering any absorptive effect. However, it has been argued that the momentum distributions might be affected substantially by the reaction process which stresses the outer region of the wave function due to the initial and the final-state interaction [6–8]. It is an interesting question to see how much the reaction mechanism affects the width of the momentum distribution and to see whether it is possible or not to draw any quantitative information on the structure of halo wave functions from these experimental data.

The momentum distributions of projectile fragments were studied extensively two decades ago for well-bound stable nuclei [9]. It is known that the momentum distributions of the fragments are well-described phenomenologically by the Gaussian shape with the width parameter σ, $\exp(-k^2/2\sigma^2)$, regardless of the fragment mass. The width parameter σ was related by Goldhaber [10] to the Fermi momentum of nucleus k_F by

$$\sigma = \sqrt{A_b(A_a - A_b)/(A_a - 1)}\sigma_0 \qquad (1)$$

where A_a (A_b) is the mass of the projectile (fragment) and $\sigma_0^2 = \langle k^2 \rangle/3 = \frac{1}{5}k_F^2$. Later, using a simple model, Friedman [6] related the width to the separation energy of removed nucleons and the absorptive cutoff, rather than the Fermi momentum. His model is based on the assumption of peripheral collision for the reaction, which works reasonably well for describing both high- and medium-energy experimental data.

Recently, a peripheral direct reaction model [11] was proposed to calculate the momentum distributions of the fragments of halo nuclei, and applied successfully to the study of the transverse momentum distributions of the reaction $^{11}\text{Be} \rightarrow {}^{10}\text{Be} + X$ using microscopic wave functions. The basic assumption of the model is a sudden approximation for the breakup process which will be realistic when the absorption is strong between projectile and target. This model resembles the Serber model [12] concerning the geometry of the reaction, while the fragmentation process is treated in a more realistic way. Very recently, a spectator model [8] was also used for the study of projectile fragmentation of halo nuclei. In the spectator model, complex optical potentials play the essential role to give the cross sections. As will be seen in Sec. II, the peripheral model in Ref. [11] has a close similarity to the spectator model in the basic reaction mechanism.

In this paper, we report the study of the projectile fragmentation of halo nuclei ^{11}Be and ^{11}Li using mainly the peripheral direct reaction model. Special focus will be on the difference between the longitudinal and transverse momentum distributions, and also the difference between the momentum distributions and a straightforward Fourier transform of the internal wave function. Furthermore, we will discuss the difference among various models for the prediction of the width of the momentum distribution. This paper is organized as follows. Section II is devoted to the formulas of the peripheral direct reaction model. Calculated results of the fragmentation cross sections are shown in Sec. III for ^{11}Be and ^{11}Li projectiles and compared with experimental data. In Sec. III, we will discuss also the Friedman model and the Serber model in comparison with the present calculations. A summary is given in Sec. IV.

II. PERIPHERAL DIRECT REACTION MODEL

The reaction process concerned is written symbolically as

$$a + A \rightarrow b + X, \qquad (2)$$

where a (A) is the projectile (target) and b is the observed fragment. The residue of the reaction is denoted as X. The transition matrix element for this process is given in the peripheral direct reaction model [11] by

$$T(\mathbf{b_x}, \mathbf{k_b}) = \int d\mathbf{r_b} \exp(-i\mathbf{k_b} \cdot \mathbf{r_b}) \psi_\alpha(\mathbf{r_b} - \mathbf{r_x}) \times \exp(i\mathbf{k_a} \cdot \mathbf{r_a}) \Theta(b_b - R_b - R_t), \quad (3)$$

where $\psi_\alpha(\mathbf{r_b} - \mathbf{r_x})$ is the wave function between the fragment b and the nucleons x in the projectile. The cylindrical coordinate $\mathbf{r} = (\mathbf{b}, z)$ is used hereafter taking the incident beam direction as the z direction. The impact parameter $\mathbf{b}$ is measured from the z axis passing the center of mass of the target. The value R_b (R_t) is the radius of the fragment (target). This formula is derived based on a sudden approximation similar to the Serber model [12]. Equation (3) can be rewritten as

$$T(\mathbf{b_x}, \mathbf{k_b}) = \int d\mathbf{r_b} \exp(i\mathbf{q} \cdot \mathbf{r_b}) \psi_\alpha(\mathbf{r_b} - \mathbf{r_x}) \times \Theta(b_b - R_b - R_t), \quad (4)$$

where $\mathbf{q} \equiv (A_b/A_a)\mathbf{k_a} - \mathbf{k_b}$. The differential cross section for the stripping reaction is given by

$$\frac{d\sigma}{d\mathbf{k_b}} = \int d\mathbf{b_x} |T(\mathbf{b_x}, \mathbf{k_b})|^2 \Theta(R_x + R_t - b_x), \quad (5)$$

where the Θ function ensures the breakup reaction to take place. The form of the absorptive cutoff depends on observables of the breakup reaction. Equations (4) and (5) correspond to the inclusive process like $^{11}\mathrm{Be} \rightarrow {}^{10}\mathrm{Be} + X$, since the cutoff $\Theta(b_b - R_b - R_t)$ represents the survival probability of the b fragment from the collision with target, while the function $\Theta(R_x + R_t - b_x)$ describes the process that X fragment interacts with the target.

In Refs. [7,8], the fragmentation cross section was formulated in the spectator model to be

$$\frac{d\sigma}{d\mathbf{k_b}} \propto \int d\mathbf{b_x} |\tilde{\phi}_a(\mathbf{q}, \mathbf{b_x})|^2 [1 - |S_{xA}(b_x)|^2], \quad (6)$$

where

$$\tilde{\phi}_a(\mathbf{q}, \mathbf{b_x}) = \int d\mathbf{r_b} \exp(i\mathbf{q} \cdot \mathbf{r_b}) \psi_\alpha(\mathbf{r_b} - \mathbf{r_x}) S_{bA}(b_b). \quad (7)$$

$S_{iA}(b_i)$ is the S matrix for the elastic scattering of the cluster i ($i = b, x$) from the target A. The S matrix changes from 0 to 1 in the surface region and the functional form will be determined by both the nature of the interaction and the surface thickness of nuclei. It is expected that the short-range character of nuclear interaction leads to a rapid change of the S matrix at the surface so that the replacement of S matrix by the Θ function is reasonable in the limit of thin surface thickness and strong absorption. Substituting the Θ functions for the S matrices, formulas (6) and (7) become identical to the corresponding ones (5) and (4) of the present peripheral model. It is an open and interesting question whether the replacement by the Θ function is still valid in the case of heavy target where the long-range Coulomb interaction contributes significantly to the breakup cross section, and whether the phase of the S matrix plays an important role or not.

III. RESULTS AND DISCUSSION

We study first the reaction $^{11}\mathrm{Be} \rightarrow {}^{10}\mathrm{Be} + X$ on targets $^{12}\mathrm{C}$ and $^{208}\mathrm{Pb}$. As the wave function ψ_α in $^{11}\mathrm{Be}$, two kinds of $2s_{1/2}$ wave functions, i.e., the halo wave function and the harmonic-oscillator wave function, are adopted. The halo wave function is calculated using a modified Hartree-Fock potential, which is adjusted to reproduce the experimental neutron separation energy in

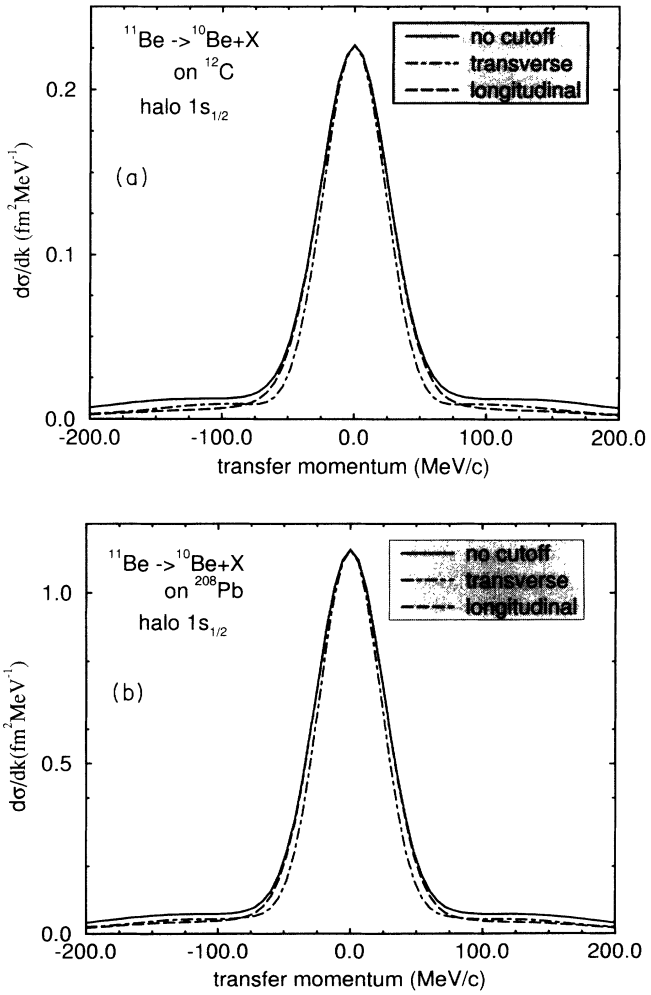

FIG. 1. Momentum distributions of the fragment $^{10}\mathrm{Be}$ from the reaction of $^{11}\mathrm{Be}$ with targets $^{12}\mathrm{C}$ (a) and $^{208}\mathrm{Pb}$ (b). The solid curve shows the result without any absorptive cutoff in Eqs. (3) and (4), while dotted and dashed curves correspond to the transverse and longitudinal cross sections obtained with the absorptive effects of both the target and the core of the projectile. The halo single-particle wave function is used for the calculation.

^{11}Be, $S_n = 0.51$ MeV [13,14]. For the harmonic-oscillator wave functions, the oscillator length b is taken as 1.52 fm which gives the empirical rms radius of ^{10}Be. The cross sections of the fragment ^{10}Be are calculated using Eq. (5) for three different cases; no cutoff, and longitudinal and transverse cross sections with the absorptive cutoff. The no cutoff cross section is obtained without Θ functions in Eqs. (4) and (5), i.e., no limit for the integrations of $\mathbf{b_x}$ and $\mathbf{r_b}$. In this case, the cross section (4) becomes identical to the straightforward Fourier transform of the internal wave function ψ_α. The calculations with the cutoff are performed by taking phenomenological radii for targets ($R_t = 2.47$ fm for ^{12}C and 5.50 fm for ^{208}Pb) and the core of the projectile ($R_b = 2.28$ fm for ^{10}Be). The finite size of neutron R_x is ignored. The Θ function acts on the transverse direction to the beam direction because of the geometry of the cutoff.

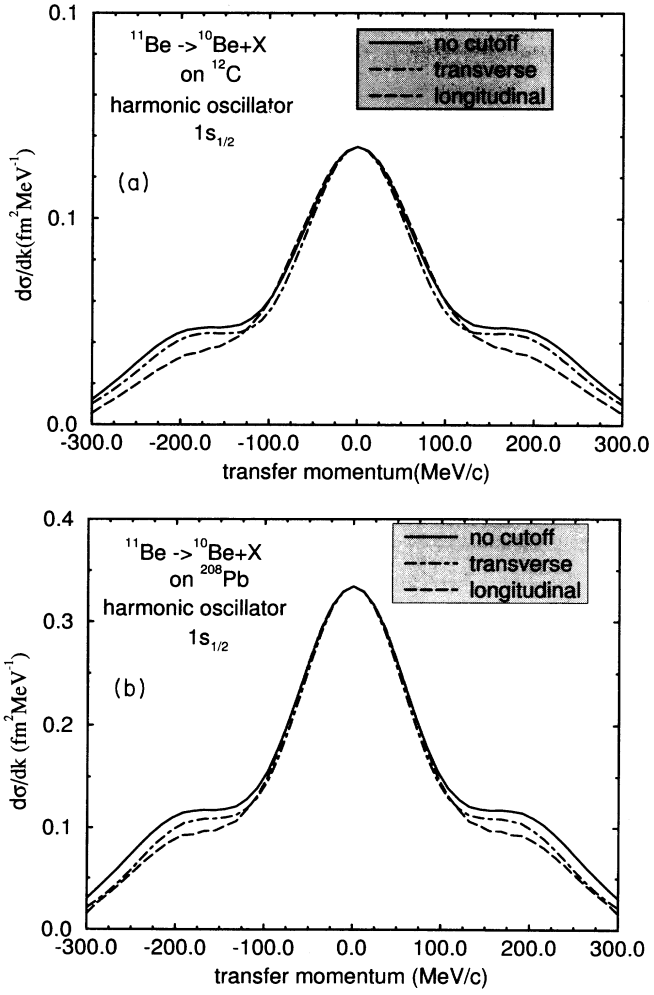

FIG. 2. Momentum distributions of the fragment ^{10}Be from the reaction of ^{11}Be with targets ^{12}C (a) and ^{208}Pb (b). The solid curve shows the result without any absorptive cutoff in Eqs. (3) and (4), while dotted and dashed curves correspond to the transverse and longitudinal cross sections obtained with the absorptive effects of both the target and the core of the projectile. The harmonic oscillator single-particle wave function with the oscillator length $b = 1.52$ fm is used for the calculation.

TABLE I. The full width at half maximum $\Gamma_{\rm FWHM}$ and the width σ (in units of MeV/c) of the momentum distributions of the inclusive reaction ^{11}Be$\rightarrow^{10}$Be+X with the targets ^{12}C and ^{208}Pb. The radii of targets are taken to be $R_t = 2.47$ fm for ^{12}C and $R_t = 5.50$ fm for ^{208}Pb. The value σ is calculated by using a formula $\sigma = \Gamma_{\rm FWHM}/2.37$ which is derived by assuming Gaussian momentum distribution.

Halo wave function with $\sqrt{\langle r^2\rangle} = 5.16$ fm				
Target	^{12}C		^{208}Pb	
	$\Gamma_{\rm FWHM}$	(σ)	$\Gamma_{\rm FWHM}$	(σ)
No cutoff	62.8	(26.5)	62.8	(26.5)
Longitudinal	62.1	(26.2)	62.3	(26.3)
Transverse	56.1	(23.7)	55.7	(23.5)

Harmonic-oscillator wave function with $\sqrt{\langle r^2\rangle} = 2.54$ fm				
Target	^{12}C		^{208}Pb	
	$\Gamma_{\rm FWHM}$	(σ)	$\Gamma_{\rm FWHM}$	(σ)
No cutoff	180.1	(76.0)	180.1	(76.0)
Longitudinal	181.8	(76.7)	176.7	(74.6)
Transverse	166.3	(70.1)	170.2	(71.8)

The calculated results are shown in Fig. 1 for halo wave function, and in Fig. 2 for harmonic-oscillator one with targets C and ^{208}Pb. The obtained widths are tabulated in Table I. The full width at half maximum $\Gamma_{\rm FWHM}$ is obtained from the calculated distributions, while the width σ in Eq. (1) is obtained from the formula [2]

$$\sigma = \Gamma_{\rm FWHM}/2.37 \tag{8}$$

assuming the Gaussian shape for the cross section around the peak.

In general, the width of the momentum distribution is not much affected by the cutoff while the absolute magnitude changes substantially. The width of the transverse momentum distribution is narrower than the longitudinal one by about 10% as is shown in Table I. As is expected, the halo wave function gives a very narrow width for the cross section compared with that for the harmonic-oscillator wave function shown in Fig. 2. The momentum distribution for the harmonic-oscillator wave function has a large tail in the region of the momentum transfer k = 100–200) MeV/c, while the cross section in high-k region is completely suppressed in the case of halo wave function. The momentum distributions of harmonic-oscillator wave functions are thus characterized not only in the peak region but also in the tail.

The results of the widths listed in Table I can be understood in general from the phase-space argument; the wider (narrower) distribution in the coordinate space gives the narrower (wider) distribution in the momentum space. One can say alternatively this effect as the result of the uncertainty principle. This physical effect gives a qualitative explanation of the difference between the transverse and longitudinal momentum distributions, and also that between the halo and the harmonic-oscillator wave functions. In the former com-

parison, the absorptive cutoff of the transverse direction suppresses the inner part of the wave function and gives effectively a larger mean-square radius for the removed particles than that of the original wave function; consequently, a smaller width for the transverse momentum distribution is achieved. In the latter comparison, it is obvious that the halo wave function has much larger radius than that of harmonic-oscillator one. This gives rise to a substantial difference in the width.

The halo wave function is simulated often by a Yukawa-type wave function

$$\psi(r) = \sqrt{2\alpha}\frac{e^{\alpha r}}{r} \tag{9}$$

with

$$\alpha = \sqrt{2\mu S_n/\hbar^2}, \tag{10}$$

where μ is the reduced mass and S_n is the separation energy of halo neutrons. The quantity σ can then be related to the separation energy assuming the Gaussian momentum dependence for the Fourier transform of Yukawa wave function [2]:

$$\sigma \approx \sqrt{\mu S_n}. \tag{11}$$

With the value $S_N = 0.51$ MeV for the neutron separation energy in ^{11}Be, formula (11) gives $\sigma = 20.9$ MeV, i.e., $\Gamma_{\rm FWHM} = 49.5$ MeV/c from Eq. (8), which is somewhat smaller than the prediction of the peripheral model in the case of ^{11}Be$\rightarrow^{10}$Be$+X$. This relation (11) should, however, be considered as a rough estimate, since the exact momentum dependence is the Lorenzian for the Yukawa wave function. The experimental width of the transverse momentum distributions of ^{10}Be is reported as $\Gamma_{\rm FWHM} = 59.3$ MeV/c for C target in Ref. [2], and also 63 MeV for Be target in Ref. [3]. These experimental values are consistent with the calculated ones in Table I. The longitudinal results are also reported in Ref. [15] to be $\Gamma_{\rm FWHM} = 43$ MeV/c, independent of targets. This data shows a somewhat smaller width than the values in Table I, while the target independence is the same with our prediction.

We show the results of our calculations for the reaction ^{11}Li$\rightarrow^{9}$Li$+X$ with targets ^{9}Be and ^{181}Ta in Fig. 3 and Table II. Several sophisticated microscopic wave functions are now available in the literature [16] for ^{11}Li. However, we adopt a simple pointlike dineutron cluster wave function (9) [17] which gives a transparent picture for the reaction mechanism than the complicated wave functions. The separation energy of the neutron halo is taken to be the empirical value $S_n = 0.31$ MeV [2]. We found a sharp peak for the longitudinal momentum distributions of the ^{9}Li fragment with the width $\Gamma_{\rm FWHM} = 46.3$ (47.0) MeV for ^{9}Be (^{181}Ta) target. The transverse momentum distributions are even narrower than the longitudinal ones similarly to those of ^{10}Be.

There are several experimental data available for the momentum distributions of ^{9}Li from the breakup of ^{11}Li.

TABLE II. The full width at half maximum $\Gamma_{\rm FWHM}$ and the width σ (in units of MeV/c) of the momentum distributions of the inclusive reaction ^{11}Li$\rightarrow^{9}$Li$+X$ with the targets ^{9}Be and ^{181}Ta. The radii of targets are taken to be $R_t = 2.38$ fm for ^{9}Be and $R_t = 5.48$ fm for ^{181}Ta. The value σ is calculated by using a formula $\sigma = \Gamma_{\rm FWHM}/2.37$.

Dineutron halo wave function with $\sqrt{\langle r^2\rangle} = 4.97$ fm				
Target	^{9}Be		^{181}Ta	
	$\Gamma_{\rm FWHM}$	(σ)	$\Gamma_{\rm FWHM}$	(σ)
No cutoff	49.9	(21.0)	49.9	(21.0)
Longitudinal	46.3	(19.5)	47.0	(19.8)
Transverse	43.4	(18.3)	42.3	(17.9)

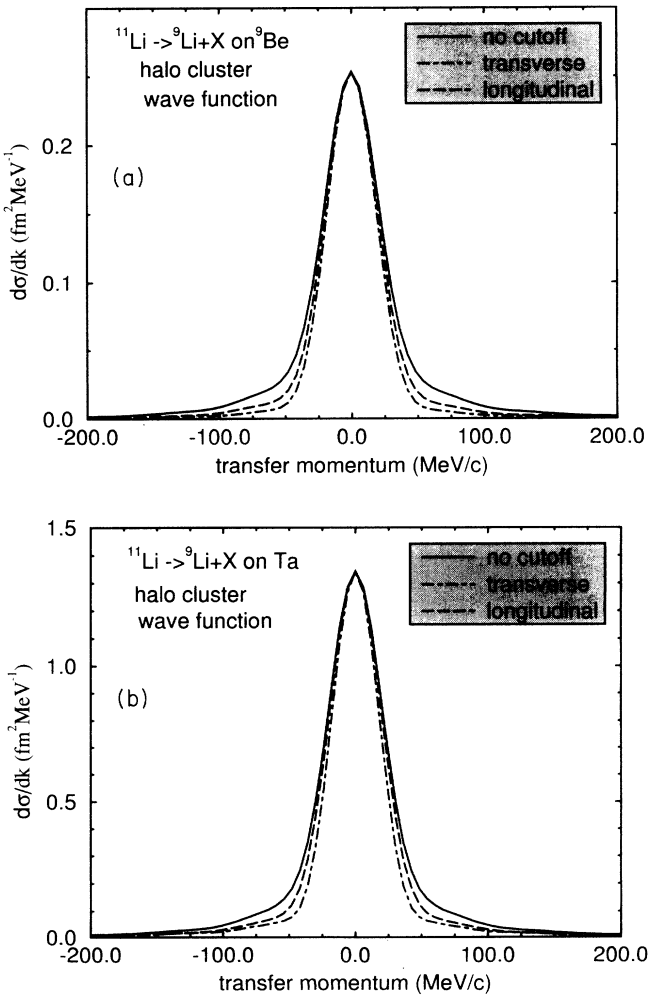

FIG. 3. Momentum distributions of the fragment ^{9}Li from the reaction of ^{11}Li with targets ^{9}Be (a) and ^{181}Ta (b). The solid curve shows the result without any absorptive cutoff in Eqs. (3) and (4), while dotted and dashed curves correspond to the transverse and longitudinal cross sections obtained with the absorptive effects of the target and the core of the projectile. The point-cluster halo wave function is used for the calculation.

The observed width $\Gamma_{\rm FWHM}$ of the longitudinal distributions are 46 MeV/c for Be and 39 MeV/c for Ta targets [4]. The former value is surprisingly close to our calculated values in Table II although we adopted the simple dineutron cluster wave function for the halo. This agreement suggests that the asymptotic behavior of the halo neutrons in ^{11}Li is crucial to describe the momentum distributions and the cluster wave function has a realistic asymptotic behavior at large distance, at least for the study of the width of the fragmentation. The correlation between two halo neutrons changes appreciably the momentum distributions [18]. Nevertheless, it is rather difficult to observe this correlation effect clearly in the experimental data because of the poor statistics. The transverse momentum distributions of ^{9}Li were also measured in various targets at various projectile energies. In Ref. [19], the width $\Gamma_{\rm FWHM}$ is observed as 37 MeV/c for C and 30 MeV/c for Pb targets at the projectile energy 280 MeV/nucleon. These values are somewhat smaller than the observed widths for the longitudinal ones, and consistent with our predictions. In the high energy case at $E_{\rm lab}$ = 790 MeV/nucleon [20], the transverse widths are observed being somewhat larger than those of the intermediate energy at $E_{\rm lab}$ = 280 MeV/nucleon.

Our calculations predict a slightly larger width of the momentum distribution than the experimental data for heavy targets. This can be understood as the effect of the Coulomb breakup, which we ignored in our calculations. The Coulomb breakup cross section of ^{11}Li through a soft dipole state was studied in Refs. [21,18]. Compared with our results, one can observe that the width of the momentum distribution in the Coulomb breakup process is smaller than that in the nuclear breakup reactions. Consequently, one can expect that the width of the momentum distribution becomes smaller if one adds the contribution of the Coulomb breakup to the nuclear breakup in the present calculations. It is thus important to include the effect of Coulomb breakup for the study of the width, especially in heavy nuclei. In the context of the present study, the effect of the Coulomb breakup can be included by a modification of the absorptive cutoff based on S-matrix theory. This study is under progress and will be published elsewhere [22].

Friedman [6] proposed a simple model to discuss the connection of the width of the projectile fragmentation to both the separation energy and the absorptive cutoff radius of projectile, rather than the Fermi momentum. His model introduced the absorptive cutoff only between the observed fragment and the residue, while the cutoff due to the target is also taken into account in the present model through the step function in Eqs. (4) and (5). Another difference is that Friedman introduced a cutoff also parallel to be beam direction. The transition amplitude of the Friedman model can be obtained from Eq. (4) by assuming a head-on collision of the fragment x with the target, i.e., $\mathbf{r_x} = 0$. Furthermore, his choice of the cutoff parameter x_0 in Ref. [6] corresponds to ignoring the size of the target R_t in Eq. (4). Despite these differences, it will be illustrative to use his model for obtaining analytic formulas of the momentum distributions. In his model, the momentum distribution is evaluated by

$$\tilde{\phi}(\mathbf{k}) = \int d\mathbf{r}\, \exp(i\mathbf{k}\cdot\mathbf{r}) F(\mathbf{r}_\perp, z)\psi_\alpha(\mathbf{r}), \tag{12}$$

where F is the absorptive cutoff perpendicular and parallel to the beam direction z. We take a Gaussian form for the absorption,

$$F(\mathbf{r}_\perp, z) = \left[1 - \exp\left(-\frac{\gamma}{2} r_\perp^2\right)\right] \exp\left(-\frac{\gamma'}{2} z^2\right), \tag{13}$$

where γ is determined by the radius of core of the projectile due to the peripheral nature of the reaction, while γ' is related to the size of reaction zone. The reaction zone itself is again determined by the peripheral nature of the reaction, and also the surface thickness. In Ref. [6], the integrand (12) is expanded around $r_\perp = R_t$ and $z = 0$ to take into account the peripheral absorptive effect as well as the finite extension of reaction zone, and the parameter γ' is described by the cutoff parameter x_0 and the radius parameter μ of the wave function. The radius parameter μ is related to the separation energy and governs the surface diffuseness of the wave function. The Gaussian form of the cutoff (13) thus includes the same effects as the expansion method in Ref. [6]. We take the wave function $\psi_\alpha(\mathbf{r})$ also as a Gaussian form:

$$\psi_\alpha(r) = N \exp\left(-\frac{\alpha r^2}{2}\right) \tag{14}$$

with the normalization factor N. The integration (12) can then be performed analytically, and the integrand is separated into two parts:

$$\tilde{\phi}(k_\parallel) \propto \exp\left(-\frac{k_\parallel^2}{2(\alpha+\gamma')}\right), \tag{15}$$

$$\begin{aligned}\tilde{\phi}(k_\perp) &\propto \exp\left(-\frac{k_\perp^2}{2\alpha}\right)\left[\frac{\alpha+\gamma}{\gamma} - \frac{\alpha}{\gamma}\exp\left(\frac{\gamma}{2\alpha(\alpha+\gamma)}k_\perp^2\right)\right] \\ &\approx \exp\left(-\frac{k_\perp^2}{2(\alpha+\gamma)}\right).\end{aligned} \tag{16}$$

One can see in Eqs. (15) and (16) that both the transverse and the longitudinal momentum distributions are affected by the cutoff in the coordinate space and the width becomes narrower than those without the cutoff. The magnitude of the effect depends on the relative magnitude of the two parameters α and γ (or γ'). These features are exactly the same as those found in the present calculations for the transverse momentum distributions.

The Serber model was first introduced to study the breakup of the deuteron [12], and modified later to analyze the cross sections of projectile fragmentation of various nuclei [23]. This model is based on the sudden approximation similar to the present peripheral direct reaction model. In the Serber model, only the absorption effect due to the target was taken into consideration and the core effect is discarded because of the deuteron projectile. A more important aspect of the Serber model is that it introduces a cutoff only in the x axis along which the neutron and the proton are aligned. The integration is cut off unless $x_n > 0$ and $x_p < 0$ measuring x from the surface of the target. For this circumstances,

the neutron misses and the proton hits the target. This is geometrically very different from our model and also from the Friedman model in which the curvature of the edge of nucleus is treated in a three-dimensional coordinate. The one-dimensional cutoff makes the fluctuation in the coordinate space smaller contrary to our way of introducing the cutoff. Consequently, the width of the momentum distribution is increased due to the cutoff in the Serber model.

IV. SUMMARY

In summary, we studied the transverse and longitudinal momentum distributions of projectile fragments of unstable nuclei ^{11}Be and ^{11}Li by using a peripheral direct reaction model. It is found that the transverse momentum distribution of the fragment is affected by absorptive cutoff of the fragmentation process, and the width becomes 10% narrower than that of no cutoff cross section. The longitudinal momentum distribution remains almost unaffected by the absorption as far as the width is concerned. The analytical formulas derived from the Friedman model show qualitatively the same features as those of the present calculations for the transverse momentum distribution. The calculated results for the reactions $^{11}\mathrm{Be}\rightarrow{}^{10}\mathrm{Be}+X$ and $^{11}\mathrm{Li}\rightarrow{}^{9}\mathrm{Li}+X$ with the halo wave functions show good agreement with experimental data at intermediate and high energies.

The momentum distributions of projectile fragments from well-bound nuclei were studied systematically 2 decades ago. Through these analyses [9], it was concluded that the momentum distribution is well simulated by the Gaussian shape $\propto \exp(-k^2/2\sigma^2)$ with a constant reduced width $\sigma_0 \simeq 80$ MeV/c irrespective of fragment mass. This constant reduced width σ_0 reflects simply the fact that the separation energy of stable nuclei are always close to 7 MeV as one can derive from Eqs. (1) and (11). For halo nuclei, the most important ingredient for the width is the asymptotic behavior of the wave function which is governed again by the separation energy. Thus, it is quite general in both stable and unstable nuclei that the width of the momentum distribution is a measure of the separation energy of the removed nucleons. However, one should carefully examine the momentum distributions of fragments using a reaction model which takes a realistic reaction mechanism into account, before making any quantitative statement on the structure of halo nucleus. This is because the separation energy of halo nucleus is one order of magnitude smaller than that of stable nucleus, and the reaction mechanism affects the momentum distribution, especially, for its transverse component.

ACKNOWLEDGMENTS

We are grateful to Professor K. Yazaki and Professor M. Ishihara for useful discussions. This work is supported by the Grant-in-Aid for General Scientific Research, Contract No. 04640280, and the Grant-in-Aid for General Scientific Research on Priority Area C. No. 05243101, for the Japanese Ministry of Education, Science and Culture.

[1] See, for example, I. Tanihata, Nucl. Phys. **A522**, 275c (1991); J. D. Garrett *et al.*, *ibid.* **A557**, 701c (1993).
[2] T. Kobayashi *et al.*, Phys. Rev. Lett. **60**, 2599 (1988); Nucl. Phys. **A538**, 343c (1992).
[3] R. Anne *et al.*, Phys. Lett. B **304**, 55 (1993).
[4] N. A. Orre, Phys. Rev. Lett. **69**, 2050 (1992).
[5] I. Tanihata *et al.*, Phys. Lett. B **287** 307 (1992).
[6] W. A. Friedman, Phys. Rev. C **27**, 569 (1983).
[7] M. S. Hussein and K. W. McVoy, Nucl. Phys. **A445**, 124 (1985).
[8] C. Bertulani and K. W. McVoy, Phys. Rev. C **46**, 2638 (1992).
[9] D. E. Greiner, P. J. Lindstrom, H. H. Heckman, B. Cork, and F. S. Bieser, Phys. Rev. Lett. **35**, 152 (1975).
[10] A. S. Goldhaber, Phys. Lett. **53B**, 306 (1974).
[11] H. Sagawa and K. Yazaki, Phys. Lett. B **244**, 149 (1990).
[12] R. Serber, Phys. Rev. **72**, 1008 (1947).
[13] G. F. Bertsch, B. A. Brown, and H. Sagawa, Phys. Rev. C **39**, 1154 (1989).
[14] P. G. Hansen, Nucl. Phys. **A553**, 89c (1993).
[15] J. Kelley *et al.*, in *Proceedings of the Third Radioactive Nuclear Beam Conference*, Michigan State University, 1993, edited by D. J. Morrissey (Editions Frontieres, Gif-sur-Yvette, 1993), p. 345.
[16] T. Hoshino, H. Sagawa, and A. Arima, Nucl. Phys. **A506**, 271 (1990); Y. Tosaka and Y. Suzuki, *ibid.* **A512**, 46 (1990); G. F. Bertsch and H. Esbensen, Ann. Phys. **209**, 327 (1991); M. V. Zhukov *et al.*, Phys. Lett. **265**, 19 (1991).
[17] A. B. Migdal, Sov. J. Nucl. Phys. **16**, 238 (1973); N. Takigawa and H. Sagawa, Phys. Lett. B **265**, 23 (1991).
[18] H. Esbensen, G. F. Bertsch, and K. Ieki, Phys. Rev. C **48**, 326 (1993).
[19] H. Humbert *et al.*, GSI Annual report, 1992.
[20] T. Kobayashi, Nucl. Phys. **A553**, 465c (1993).
[21] H. Esbensen, Phys. Rev. C **44**, 440 (1991).
[22] M. Ueda, H. Sagawa, and N. Takigawa, unpublished.
[23] H. Utsunomiya, Phys. Rev. C **32**, 849 (1985).

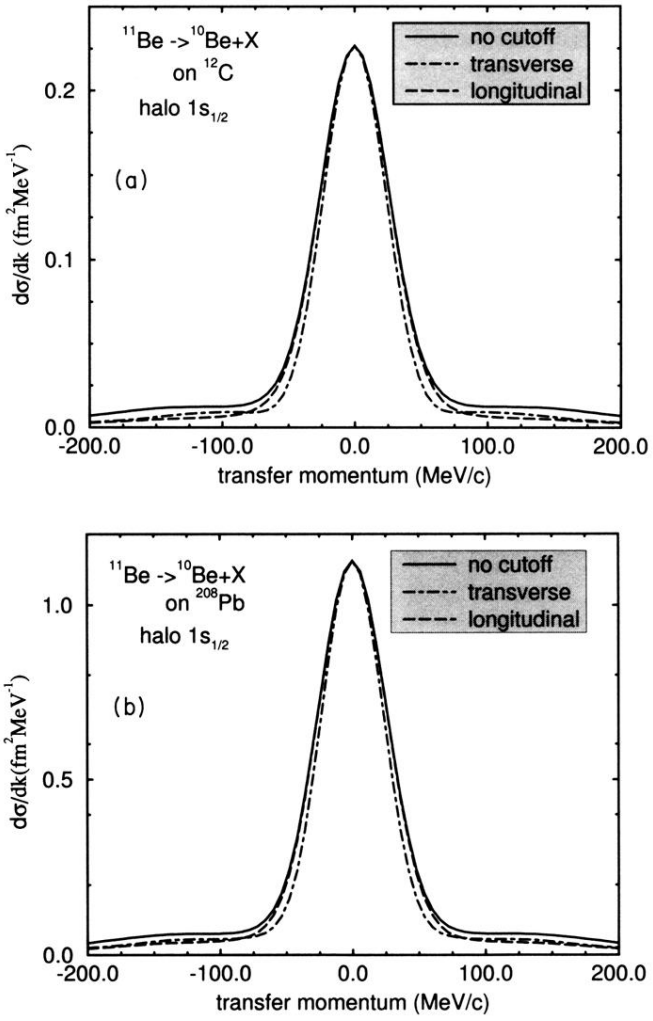

FIG. 1. Momentum distributions of the fragment ^{10}Be from the reaction of ^{11}Be with targets ^{12}C (a) and ^{208}Pb (b). The solid curve shows the result without any absorptive cutoff in Eqs. (3) and (4), while dotted and dashed curves correspond to the transverse and longitudinal cross sections obtained with the absorptive effects of both the target and the core of the projectile. The halo single-particle wave function is used for the calculation.

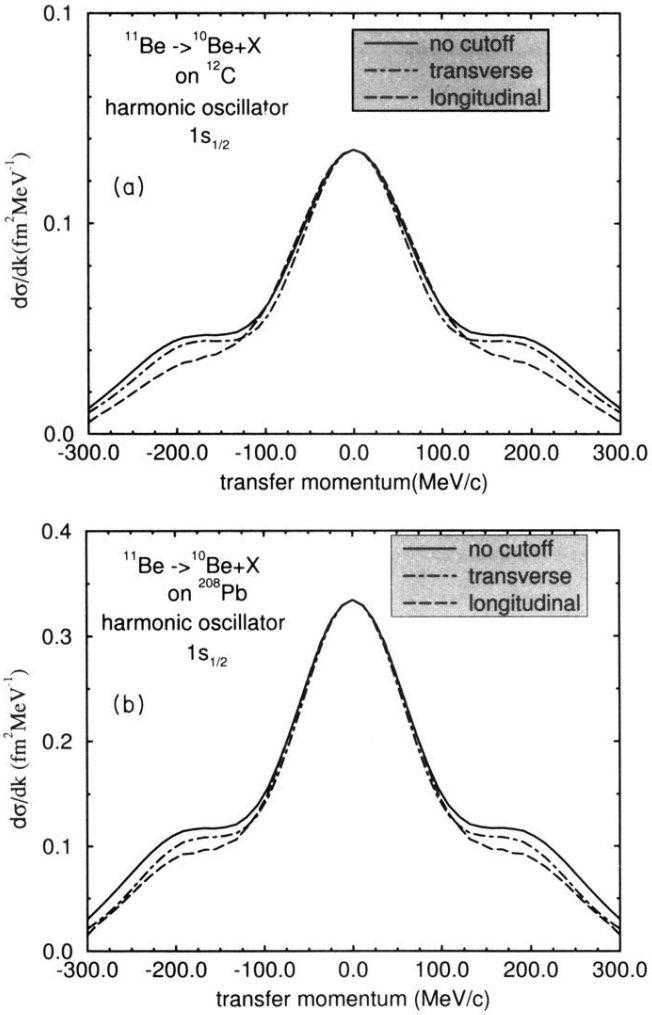

FIG. 2. Momentum distributions of the fragment ^{10}Be from the reaction of ^{11}Be with targets ^{12}C (a) and ^{208}Pb (b). The solid curve shows the result without any absorptive cutoff in Eqs. (3) and (4), while dotted and dashed curves correspond to the transverse and longitudinal cross sections obtained with the absorptive effects of both the target and the core of the projectile. The harmonic oscillator single-particle wave function with the oscillator length $b = 1.52$ fm is used for the calculation.

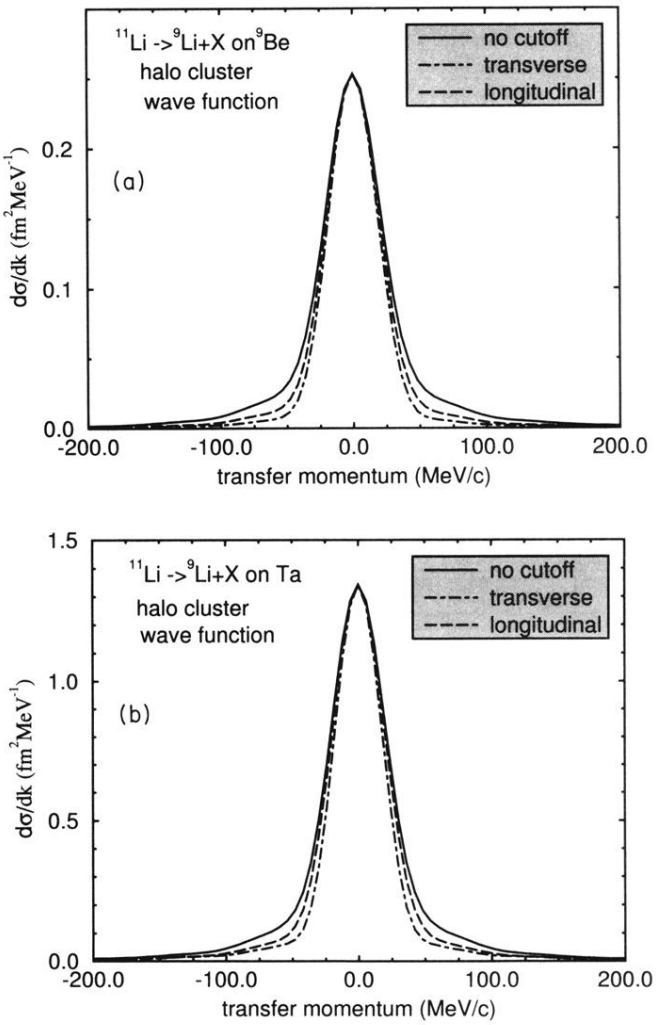

FIG. 3. Momentum distributions of the fragment ^{9}Li from the reaction of ^{11}Li with targets ^{9}Be (a) and ^{181}Ta (b). The solid curve shows the result without any absorptive cutoff in Eqs. (3) and (4), while dotted and dashed curves correspond to the transverse and longitudinal cross sections obtained with the absorptive effects of the target and the core of the projectile. The point-cluster halo wave function is used for the calculation.